Chapter 3

Optimal Placement of Sensors and Actuators for Feedforward Noise and Vibration Control

Thomas Haase

Additional information is available at the end of the chapter

http://dx.doi.org/10.5772/64409

Abstract

Active systems for noise and vibration control have been under investigation for more than three decades now. It is well-known that the placement of both sensor and actuator is of crucial importance for the achievement of a reasonable noise and vibration reduction. By measuring a reference signal, a feedforward control system is able to reduce even broadband stochastic excitations. Using a simple vibration control example, this chapter summarises and analyses the parameters that influence the noise and vibration reduction of a feedforward control system. Furthermore, an optimisation tool for the placement of actuators and sensors of a feedforward control system is introduced. A special emphasis is placed on the analysis of the impacts of causality and the number of filter weights on the actuator placement. It can be shown that the actuator placement for a feedforward control system is dependent on the delays, the filter weights and even on the structural damping of the system. Besides the simulation results, the dependency of the actuator placement on the filter weights is experimentally investigated on a simple aluminium plate. The simulation results could only be partially validated at this stage due to model uncertainties.

Keywords: optimisation, feedforward control, noise and vibration reduction, causality, signal processing

1. Introduction

The research into the control of noise and vibration has been conducted for several decades now. A major concern of many research studies is the placement of sensors and actuators to optimise the system's performance [1–3]. A lot of metrics for sensor and actuator placement have been studied. Mainly, two approaches can be classified: First, the controllability- and

observability-driven sensor and actuator optimisation, which is mainly based on the eigenvectors and eigenfrequencies of the structure [4, 6], and, secondly, the development of an optimisation tool that couples an optimiser and a detailed controller simulation during the optimisation [7, 8].

According to the most recent literature, the active system used to calculate the cost function of the optimisation can be either a feedforward or a feedback control system [16, 31]. With regard to feedback control, several optimisation chains can be found in which the actuator and sensor positions are optimised simultaneously with several controller parameters (e.g. weighting matrices, feedback gain). Regarding feedforward controllers, only very simple control laws are used to calculate the cost function, for example, linear quadratic optimal control theory [9–11]. However, this simple control law does not incorporate the limitations of an experimentally realisable feedforward controller into the optimisation. This would be important because aspects such as causality, finite impulse response (FIR), filter length and saturation can limit the performance of a feedforward control system.

That is why this chapter first summarises the limitations of a feedforward controller, and, secondly, explains the relevant parameters for the design of such controllers. Furthermore, this study investigates the optimisation of sensor and actuator positions for feedforward controllers. By reviewing the limitation parameters of a feedforward control system and knowing that the actuator and sensor placement has an influence on all these parameters, the following question arises: How much influence does each of these parameters have on the actuator and sensor placement? To answer this question, the optimisation tool presented here allows the optimisation of sensor and actuator positions with respect to causality and filter length. Through the variation of the causality conditions and the filter weights during the optimisation of an actuator position, the relevance of these parameters for an active vibration control (AVC) system can be shown.

This chapter is structured as follows: First of all, the experimental test bed and the simulation model are presented to give an impression of the investigated system. Secondly, the parameters that are likely to influence the feedforward controller performance are presented and analysed in detail. The next section introduces the optimisation tool and shows how optimised sensor and actuator positions can be derived specifically for feedforward control systems. The last major section discusses the simulation and experimental results. Finally, a conclusion and an outlook for future research are presented.

2. Simulation model and experimental test bed

The simulations and experiments are conducted on a simple aluminium plate mounted on its four corners (with an offset of 35 mm from the corners in x- and y-direction). An aluminium plate seems to be a very simple system, but can actually be used to easily reproduce the presented results. The system model is described by the eigenvectors and eigenfrequencies of the plate calculated with a finite element (FE) simulation in ANSYS® with an undamped modal analysis. The structural properties used in the FE simulation are presented in **Table 1**.

http://dx.doi.org/10.5772/64409

Parameter	Property (Unit)	Parameter	Property (Unit)
Young's modulus	70 (GPa)	Element size	0.01 (m)
Poisson's ratio	0.34 (–)	Density	2700 (kg/m^3)

Table 1. Material properties of the FE simulation.

The damping properties of the model are defined by modal damping ratios. For the simulations presented here, a light damping ratio of 0.5% and a medium damping of 2.5% are used. A good description of the derivation of the transfer functions with the calculated eigenfrequencies, eigenmodes and damping ratios can be found in textbook [32]. The plate is not a complex structure like, for example, an aircraft fuselage, but is only used to generate the different transfer functions that can be easily reproduced. Indeed, by using a simple aluminium plate with different damping conditions, a variety of transfer functions can be evaluated. The size of (800 × 600 × 3) mm^3 enables a high modal density of up to 38 eigenfrequencies in the investigated frequency range from 1 up to 600 Hz. From a system theory point of view, the light damping configuration is a classical resonant system, for example, a generator housing or a fuselage panel. In contrast, the medium damping configuration is more comparable to the acoustic room responses presented, for example, by Kuo and Morgan [13]. Therefore, it can be stated that the presented study can be transferred to a lot of practical technical systems. Furthermore, these different configurations are investigated because the literature shows that the damping of a structure itself seems to be of importance for a feedforward controller [15].

The actuators used in this study are piezoelectric patch actuators from PI ceramics (DuraAct® P876.A12 [33]), which are widely used in active control systems. They are modelled with modal-based correction routines in such a way that the mass and the stiffness of the actuators are integrated into the structural model. Detailed information about the actuator coupling is given in [24].

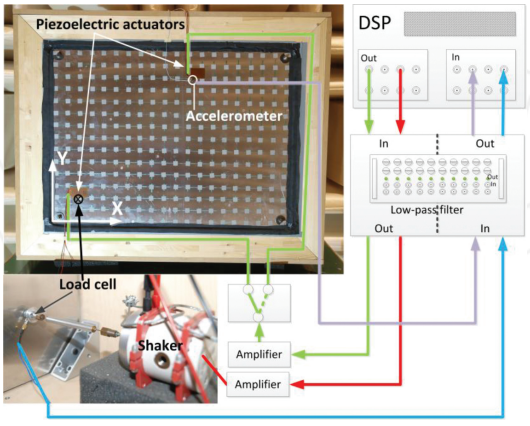

Figure 1. Experimental test bed.

For the experiments, a wooden mock-up is built to clamp the plate at its four corners. For the realisation of the medium damping, the aluminium plate is damped with constraint layer damping (CLD) from 3M®. The CLD is applied to the aluminium plate's entire rear side. A picture of the experimental test bed is given in **Figure 1**.

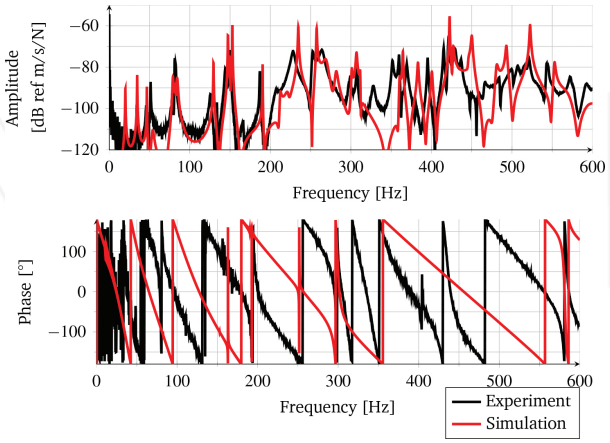

Figure 2. Bode diagram of the lightly damped secondary path.

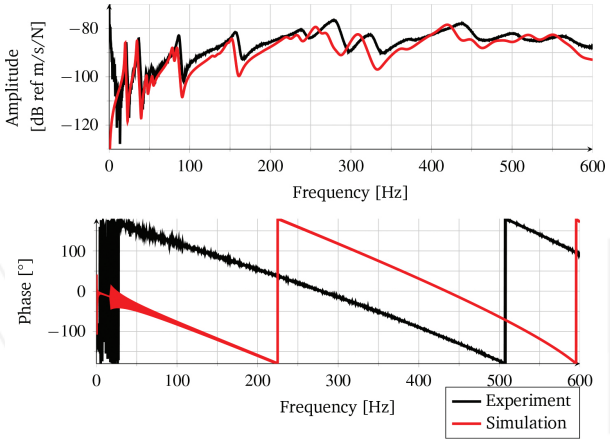

Figure 3. Bode diagram of the medium damped secondary path.

To validate the simulation model, **Figures 2** and **3** show the simulated and measured transfer paths of a piezoelectric patch actuator to an accelerometer for both damping conditions. It has to be mentioned that the phase plots of the bode diagrams only show the all-pass part of the secondary paths. The all-pass part is relevant to show the delay induced by the secondary path,

http://dx.doi.org/10.5772/64409

while the minimum-phase part describes the phase jumps of the resonant system. The derivation of the all-pass part and the minimum-phase part of a transfer function is described in detail in [19].

Figure 2 shows that the eigenfrequencies of the lightly damped model and the curve shape are well approximated, at least the damping ratio of the simulation seems to be a bit too low. The phase response is also well approximated, regardless of the phase offsets which are in deed not relevant. The gradient of the phase response is more important because it describes the group delay of the secondary path. Above 350 Hz there is a small deviation of the gradient. The simulation model of the medium damping configuration fits the experimental model up to 300 Hz, which can be seen in **Figure 3**. Above 300 Hz, there are some deviations in the transfer path. These are caused by the simplified modelling with modal damping ratios. Furthermore, the influence of the mass and stiffness of the CLD is completely neglected during the simulation.

There are mainly two reasons why the modelled transfer paths are not modelled in more detail. The first reason is that the presented deviations are usual if the system optimisation is done in a pre-design stage and, second, for more precise structural models, a model updating or an experimentally identified structural model are necessary. Furthermore, the delays and the number of filter weights needed for modelling the structure are not very sensitive towards the accurate modal frequencies.

3. Feedforward control systems

Feedforward control systems are widely used in research [3, 12, 16] and industrial projects [17, 18]. The following subsections provide a brief introduction into the theory of feedforward controllers as well as a presentation of the calculation of an optimal causal feedforward controller [14, 19]. Afterwards, the fundamental parameters influencing the performance of a feedforward controller are described. The section closes with the presentation of the results of a huge parametric study conducted on different control set ups.

3.1. Fundamentals of feedforward control

The most common realisation of a feedforward controller is the adaptive filtered-x least mean square algorithm. The advantages of an adaptive feedforward controller are their stability (90° phase margin) and their robustness (adaptive algorithm) [13]. The analysis and description of an adaptive feedforward controller is excluded here because textbooks are available for this topic [13, 19, 25].

For stationary and ergodic excitations, the adaptive feedforward controller converges to the optimal Wiener solution [19]. Therefore, the optimal feedforward controller is used in this chapter because it is not possible to wait for the convergence of an adaptive algorithm during an optimisation.

A typical block diagram of a feedforward control system is presented in **Figure 4**. The classical feedforward controller is used to cancel a disturbance signal $d(n)$ by filtering a reference signal $x(n)$ with a filter W and the secondary path G. The secondary path G represents the dynamics of the technical system used to counteract the disturbance signal through the secondary signal $y(n)$. In the technical system presented in **Figure 1**, the secondary path is described by the reconstruction low-pass filter, the piezoelectric patch actuator, the aluminium plate, the accelerometer and the anti-aliasing filter. The primary path P describes the dynamics between the reference signal and the disturbance signal and is typically unknown in technical applications. The advantage of a feedforward controller over a feedback controller lies in the possibility to measure a time-advanced reference signal, which allows counteracting even stochastic broadband disturbances. Time-advanced means that the travelling disturbance wave (acoustic or structural bending wave) is first measured by the reference signal and after a specific delay by the disturbance or error sensor.

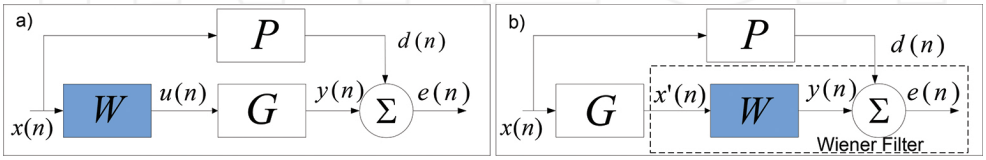

Figure 4. Block diagram of a feedforward controller: (a) classical scheme, (b) filtered reference signal scheme.

3.2. Optimal causal feedforward controller

The derivation of a causal feedforward controller is described in detail in [19]. So, only a brief summary for a single-input single-output (SISO) system is given here.

Assuming that the secondary path G and the FIR realisation of the filter W are linear and time-invariant, the chronology can be reversed as presented in **Figure 4(b)**. As can easily be seen, the classical Wiener filter theory can now be used to calculate the optimal filter for a quadratic cost function of the error signals

$$J = E[e^2(n)]. \tag{1}$$

The only step that has to be done is the calculation of the filtered reference signal $x'(n)$. The calculation of the filtered reference signal is explained by Eq. (2) in which the secondary path G is realised by a FIR filter. Of course, this is only one possibility as the secondary path can also be realised by a state-space model

$$x'(n) = \sum_{i=0}^{L-1} g_i \cdot x(n-i) \tag{2}$$

In Eq. (2), g_i describes the i-th bin of the secondary path FIR filter of length L. Referring to the Wiener filter theory [19], the optimal controller can be calculated by

http://dx.doi.org/10.5772/64409

$$\boldsymbol{w}_{opt} = \frac{\boldsymbol{r}_{x'd}}{\boldsymbol{R}_{x'x'}}, \tag{3}$$

in which $r_{x'd}$ is the cross-correlation vector of the filtered reference signal and the disturbance signal and $R_{x'x'}$ is the autocorrelation matrix of the filtered reference signal. The calculations of both the autocorrelation matrix and the cross-correlation vector are causal as long as only past samples are used to calculate them. The autocorrelation matrix is defined by

$$\boldsymbol{R}_{\boldsymbol{x'x'}} = \begin{bmatrix} r_{x'x'}(0) & r_{x'x'}(1) & \cdots & r_{x'x'}(I-1) \\ r_{x'x'}(1) & r_{x'x'}(0) & \cdots & r_{x'x'}(I-2) \\ \vdots & & & \vdots \\ r_{x'x'}(I-1) & & \ddots & r_{x'x'}(0) \end{bmatrix}, \tag{4}$$

where I is the FIR-filter length and $r_{x'x'}(m)$is the symmetric autocorrelation function of $x'(n)$ that is defined by

$$r_{x'x'}(m) = E[x'(n)x(n-m)]. \tag{5}$$

The cross-correlation vector of $x'(n)$ and $d(n)$ is defined by

$$\boldsymbol{r}_{\boldsymbol{x'd}} = [r_{x'd}(0) \quad r_{x'd}(1) \quad \cdots \quad r_{x'd}(I-1)], \tag{6}$$

in which $r_{x'd}(m)$ is defined for real and stationary time sequences by

$$r_{x'd}(m) = E[x'(n-m)d(n)]. \tag{7}$$

In summary, for the calculation of the optimal causal filter $\boldsymbol{w}_{\text{opt}}$, it is necessary to measure or simulate:

- a secondary path model and
- synchronous time series of the reference signal $x(n)$ and the disturbance signal $d(n)$.

With the mentioned data, the filter can be calculated offline and then be implemented into the digital control system or used in the optimisation routine.

3.3. Parameters of a feedforward controller

As long as it is possible to measure a time-advanced reference signal, a feedforward control system is able to achieve a broadband error signal reduction in the presence of a broadband stationary random disturbance [13]. If the time-advance of the reference signal is larger than the delays of the secondary path, then the signal processing system is called causal. Therefore, the causality constraint describes if the time-advanced reference signal is sufficient to establish a causal or a non-causal system [13]:

$$\tau_P \geq \tau_G + \tau_\Delta \tag{8}$$

Eq. (8) is defined by the primary delay τ_P, the secondary path delay τ_G, and the signal processing delay τ_Δ. While a causal system fulfils Eq. (1), a non-causal system does not fulfil the equation. In the case of a non-causal system realisation, the performance of a feedforward controller is limited. So, to accurately simulate the performance of a feedforward controller, a causal control law, as described in Section 3.2, is necessary.

The performance of a feedforward controller is also determined by the representation of the filter W. Typical representations are finite impulse response filters and infinite impulse response (IIR) filters. Details about both filter representations can be found in [19] and [20]. Here, the FIR filter representation is used because of its inherent stability and also for its easy applicability for adaptive controllers.

In summary, a lot of research papers investigate feedforward control systems regarding the effects of:

- causality [15, 21, 22],
- damping [15],
- saturation [19],
- filter weights [15],
- the number of sensors and actuators [23] and
- coherence.

The references mentioned here study several effects of a feedforward control system separately. Regarding coherence, this study neglects limitations induced by a limited coherence because a high coherence is a requirement for the use of a feedforward controller. In this study, it is assumed that the coherence is approximately 1 during the experiments.

To understand all the mentioned parameters and their influence on the performance of a feedforward control system, a large parametric study has been conducted for the AVC system presented in Section 2. To the author's best knowledge, no parametric study has been published so far, which covers such a huge range of parameter variations.

3.4. Analysis methods for feedforward control systems

This section presents a small set of metrics for the analysis of feedforward control systems. These metrics are used to interpret both the parametric study and the optimised actuator positions.

First of all, a simple metric for the performance of a feedforward control system has to be defined. For reasons of simplicity, the reduction of the vibration error signal is used. Therefore, the power of the error signal in the uncontrolled state is subtracted from the controlled state

http://dx.doi.org/10.5772/64409

$$L_{\Delta Vib} = 10 \cdot log_{10}\left(\Phi_{Tot}^{On}\right) - 10 \cdot log_{10}\left(\Phi_{Tot}^{Off}\right) = 10 \cdot log_{10}\left(\frac{\Phi_{Tot}^{On}}{\Phi_{Off}^{tot}}\right), \tag{9}$$

where Φ_{Iot} is the frequency-weighted sum of the power spectrum of the error signal

$$\Phi_{Tot} = \Delta F \cdot \sum_{n=1}^{N_L} \Phi_{ee}(n \cdot \Delta F). \tag{10}$$

The power spectrum $\Phi_{ee}(n \cdot \Delta F)$ is calculated through the "Welch method" (Welch's averaged periodogram). In the case of systems with more than one error signal, the separate error signal spectra are averaged so that the result can be used for the calculation of the total reduction.

To analyse the length of the FIR filter and to decide whether it is sufficient to model the impulse response, the filter quality is introduced. The filter quality is defined by

$$F_Q = \frac{\sum_{i=1}^{I} |w_{opt}(n)|}{\sum_{i=1}^{I_{Ref}} |w_{opt}(n)|} \cdot 100. \tag{11}$$

The filter quality is a ratio between a reference filter of sufficient length and a shortened version of the reference filter. If the optimal filter has a short impulse response the values of F_Q are large for short filter length and if the optimal filter has a long impulse response large values of F_Q are only reached for large filter lengths.

Furthermore, as presented in Subsection 3.3, the analysis of Eq. (8) requires the derivation of the delays. This can be done by analysing the all-pass part of the measured or of the simulated transfer functions [21]. Thus, in this study the group delay [19] of the all-pass part is analysed, which can be approximated by the difference quotient and is defined by

$$\tau(j\omega) = \frac{d\varphi(j\omega)}{d\omega} \approx \frac{\varphi(j\omega_N) - \varphi(j\omega_{N-1})}{\omega_N - \omega_{N-1}}. \tag{12}$$

3.5. Parametric study

3.5.1. Ranges of the investigated parameters

For the parametric study, three sensors, one piezoelectric patch actuator and one disturbance force were placed on the aluminium plate to study different sensor, actuator and disturbance configurations. At this stage of the study, the placement of the elements is unimportant because the causality is varied with synthetic delays.

To study the effects of causality, damping, filter weights and saturation on the system performance, a simple system is studied first. The positions of the shaker, the actuators and, the sensors are shown in (**Figure 5**). The aluminium plate is excited by the single point force F1, which is also taken as the reference signal, and the error signal is measured at the single

accelerometer S1. The secondary signal is induced via the piezoelectric patch actuator A1. The sampling frequency of the investigated system is 1200 Hz, so that the investigated bandwidth is from 1 to 600 Hz. **Table 2** presents the variations of the investigated parameters.

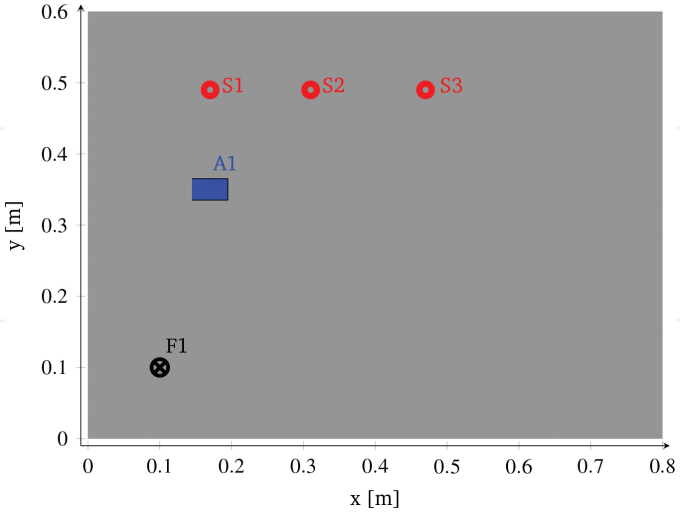

Figure 5. Configuration of sensors, actuator and disturbance source for the parametric study.

Property	Values
Unit sample delays β	0, ±1, ±2, ±3, ±6, ±12, ±18, ±24, ±36, ±48, ±72, ±96, ±192, ±384, ±1000, ±1300
Filter weights I	50, 100, 200, 300, 450, 600, 900, 1200, 1800, 2400, 3000, 3600, 4800
Modal damping ratio	0.5%, 2.5%
Saturation	100 V, 500 V, unlimited

Table 2. Parameter values.

To investigate different causality properties of the system, the primary or secondary path is additionally delayed by a number (β) of unit samples. In **Table 2**, a positive sign means that the primary path is delayed, meaning that the reference signal is more time-advanced. A negative sign represents a delay in the secondary path, meaning that the reference signal has a time penalty.

3.5.2. Results of the parametric study

In **Figure 6**, the vibration reduction $L_{\Delta Vib}$ is presented on the z-axis. The number of unit delays and the filter weights are presented on the x- and y-axis. At this stage, no saturation of the actuator voltage is introduced, which means that an unlimited voltage could be applied to the

http://dx.doi.org/10.5772/64409

piezoelectric actuator. Furthermore, the actuator is assumed to be linear even for very high amplitudes.

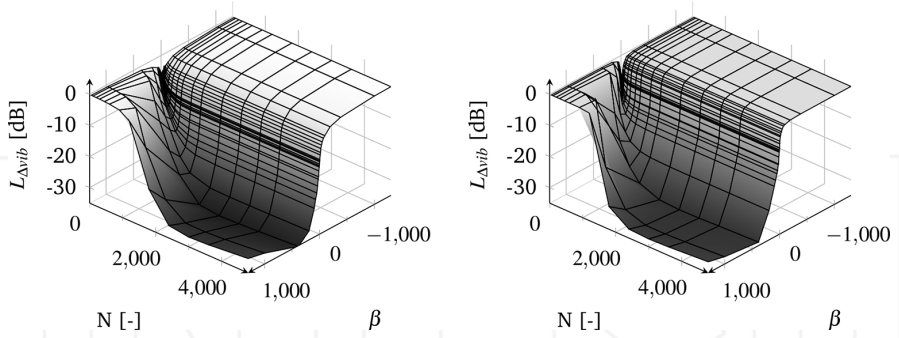

Figure 6. Total vibration reduction of the control systems with low damping (left) and medium damping (right) and no saturation.

It can be seen that in both damping configurations there is a large dependency of the vibration reduction performance on the filter weights and the delays. First of all, the lightly damped case on the left is analysed in more detail. It can be seen that even in the case of a large negative delay β, a small vibration reduction can be achieved. This is due to the lightly damped resonances that filter the stochastic force excitation towards a more deterministic signal dominated by the resonance frequencies. It can also be seen that the performance is saturated at a certain β (ca. 350), and at a large number of filter weights (ca. 1600). It should also be noticed that for small delay variations the performance is saturated at a smaller number of filter weights.

In the case of medium damping, the observed tendencies are almost identical. A major difference can be seen for negative delays, where nearly no performance is achieved. This is due to the damped resonances, which now filter the stochastic disturbances less effectively. In contrast to [15], an increased structural damping does not lead to a limitation of the performance if the feedforward controller fulfils the causality constraint.

If the actuator voltages are saturated, the overall performance is limited despite the use of a large positive delay or a large number of filter weights. **Figure 7** presents the performances for two different voltage limitations. A voltage limitation has the effect of a large performance cut-off at a certain level. For the medium damping configuration, the limitation is even more important because of the larger actuator amplitudes that are necessary to compensate the dissipated energy reasoned by the higher structural damping. If it is necessary to saturate the actuator voltage due to some design specifications (e.g. weight, size or cost), the feedforward controller, as a consequence, can be designed with shorter filters or smaller time-advances. This information is very important in designing and selecting actuators and digital signal processing (DSP) systems for feedforward control systems to reduce the overall cost and weight of such systems.

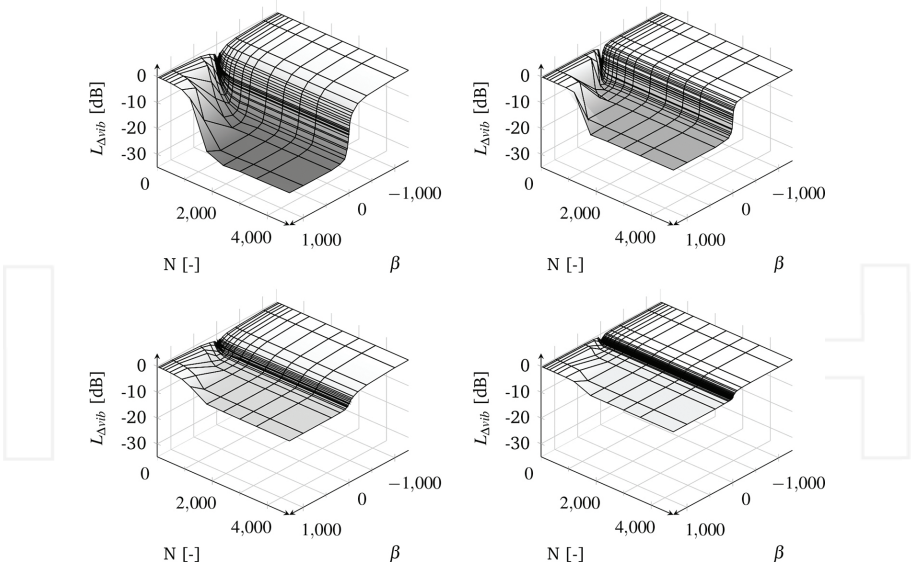

Figure 7. Total vibration reduction of the control systems with low damping (left) or medium damping (right) and a 500 V (top line) or 100 V (bottom line) limitations.

The integration of an actuator limitation is adverse, but the use of a rectangular system (more sensors than actuators) is even more dramatic for the controller performance. If the control system has to control two or three sensor positions, the performance is very limited, as presented in **Figure 8** for the lightly damped system. The introduction of a second sensor limits the performance on a scale comparable to a voltage limitation of 100 V.

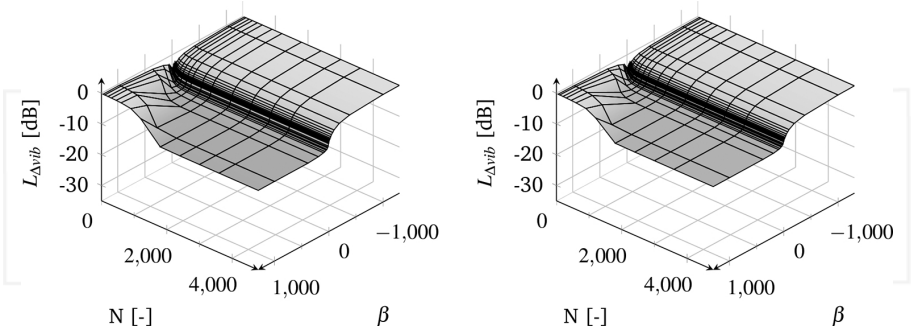

Figure 8. Total vibration reduction of the lightly damped control system with sensors S1 and S2 (left) and with sensors S1, S2 and S3 (right).

The same behaviour can be observed for the system with medium damping. The performance reduction of rectangular systems is also described in detail in [23].

http://dx.doi.org/10.5772/64409

If we now consider the actuator and sensor placement, it is easy to understand that the actuator and sensor placement determines the delays, the saturation (via controllability of the structure) and also the impulse responses of the primary and secondary path. Yet, by implication it is obvious that the feedforward controller parameters have an impact on the actuator and sensor placement. Therefore, the mentioned parameters are integrated in the actuator and sensor placement.

4. Sensor and actuator placement

The placement of sensors and actuators is important for the achievement of a sufficient performance of a feedforward control system. It is even more important than the type of actuator or sensor used in an active system [29]. For this reason, during the last decades numerous works on the optimisation of actuator and sensor placement have been published, e.g. see [1, 2] and various textbooks [19, 32]. Apart from the actuator and sensor placement including controllability and observability criteria, many researchers focus on a system design that combines genetic optimisation and a control law. These studies show that by using this particular system design method, the performance of a noise and vibration controller can be further improved. As a consequence, this chapter presents an optimisation routine that uses a genetic algorithm and a causal feedforward controller to optimise sensor and actuator locations. The following example of an actuator optimisation shows the influence of the parameters discussed in Section 3 on the actuator placement.

4.1. Optimisation tool

To efficiently design a feedforward system, an optimisation needs to be coupled to a realistic controller simulation. So the German Aerospace Center (DLR) developed an optimisation chain, which is presented in **Figure 9** as a flow chart.

Beside the initialisation of the excitation and the structural model, the two most important elements are the genetic optimisation routine and the calculation of the fitness function with a causal controller. These elements have to be initialised with several parameters, for example, number of sensors and actuators, the cost function and the parameters of the genetic algorithms. Therefore, a brief description of the genetic algorithm is given here. The genetic optimisation is of stochastic nature and based on Darwin's principle 'survival of the fittest'. A random population of individuals (e.g. actuator and sensor positions) is evaluated with a fitness function. The fitness function can be the local or global vibration reduction or the sound power reduction. In this study, the local vibration reduction is considered. This cost function is of relevance if the vibration at a specific location should be reduced, for example, at a mounting point to reduce vibration transmission [28]. Another example for a local reduction is a classical active noise control (ANC) system where the sound pressure at a microphone is reduced. After all individuals have been evaluated by the cost function they are ranked, selected, recombined and mutated to set up a new population, which again is evaluated. The genetic algorithms for ranking, selection, recombination and mutation are inspired by nature

and meant to improve each new population compared to the old one. In this study, the genetic optimisation was aborted after 50 populations and every optimisation was performed three times to avoid singularities.

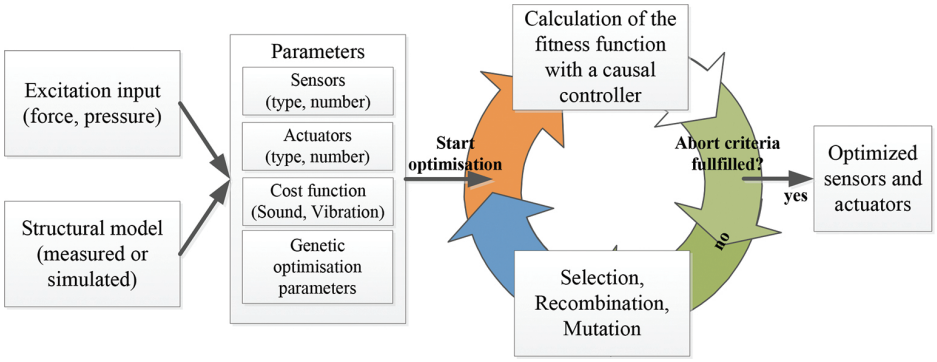

Figure 9. Flow chart of the optimization tool.

Property	Value	Property	Value
No. populations	50	Selection rate	80%
No. individuals	120	Ranking pressure	2
Mutation rate	20%	Selection mode	Stochastic universal sampling
Insertion rate	50%	Recombination	Linear

Table 3. Parameters of the genetic algorithms.

The genetic optimisation parameters are summarised in **Table 3**. Further, details about the genetic optimisation routines can be found in the manual of the genetic algorithm toolbox (GEA toolbox) [27] and in [26].

The second important element of the optimisation chain is the introduction of a causal feedforward controller. Therefore, all limitations (causality, filter weights and saturation) are integrated into the optimisation of the sensor and actuator positions. Furthermore, the delays induced by the analogue and digital signal processing units are also integrated into the simulation, as described in [21]. All signal processing elements which are relevant for the investigated system are shown in **Figure 1**. In summary, these are the anti-aliasing and reconstruction filters, the DSP, the sensors and the amplifiers. As presented in [21], the filter delays and the DSP delay are the most important, while the delay of the amplifiers and sensors is negligible. To summarise, the simulation of the feedforward controller is harmonised with the experimental realisation of a feedforward controller. The derivation of the causal controller has already been described in Section 3.2.

http://dx.doi.org/10.5772/64409

4.2. Actuator optimisation

In the following optimisation, the actuators are optimised to reduce the flexural vibration at a fixed error sensor position (S3 in **Figure 5**). The error sensor is fixed to facilitate the analysis of actuator position. The investigation focuses on the influence of causality, filter weights and the structural damping. To study the influence of causality, two different control systems are investigated:

- A non-causal system (NCS): The feedforward controller is designed with a simplified secondary path G*, where only the structural dynamics of the aluminium plate without any analogue and digital signal processing delays are integrated. For the controller design, the reference signal $x(n)$ and a delayed version of the disturbance signal $d(n)$. are used. The additional delay of the signal is 20 samples, which is sufficient to realise causal systems all over the plate for the chosen error sensor position.
- A causal system (CS): The feedforward controller is designed with the secondary path G that includes all filters, etc., the reference signal $x(n)$ and the disturbance signal $d(n)$.

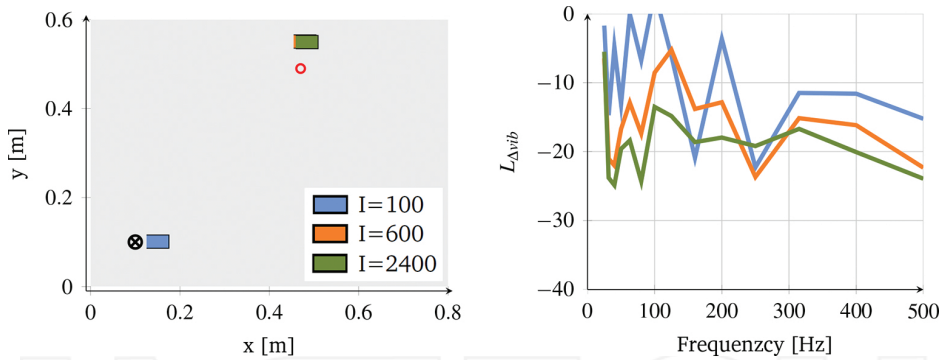

Figure 10. Optimised actuator positions for the causal system (left), vibration reduction at the error sensor in third octave bands (right).

In addition to the causality aspect, three different filter lengths (100, 600 and 2400) are used in the optimisation. The effects of a voltage limitation are investigated via the variation of the maximum actuator voltage: no limitation and 100 and 500 V limitations.

Figures 10 and **11** show the optimised actuators for the control systems with different filter lengths and different delays. By comparing **Figures 10** and **11** it can be easily seen that the actuator positions as well as the third octave vibration reduction differ significantly.

The optimised actuators of the NCS are located near the excitation for all filter weights. In contrast, the actuators of the CS are located near the error sensor except for the actuator optimised with a filter length of ($I = 100$). The CS actuators with a filter length of 600 and 2400

are nearly collocated, but the predicted performance differs by 5–10 dB in several third octave bands. This result matches with Section 3.5., where the influence of the filter weights on the vibration reduction is similar. Yet, it also shows the importance of including the filter length into an optimisation to improve the prediction accuracy. However, the different actuator placements need to be explained not only by the filter weights but rather by a combination of causality and filter weights.

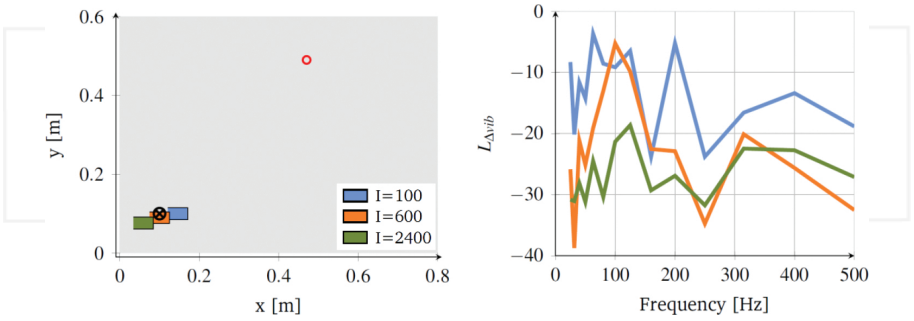

Figure 11. Optimised actuator positions for the non-causal system (left), vibration reduction at the error sensor in third octave bands (right).

To explain the actuator placement in more detail, the filter quality and the delays of the primary and secondary path are analysed. The filter qualities of the three actuator positions of the NCS are presented in **Figure 12** and those of the CS system in **Figure 13**. **Figure 11** shows different actuator positions of the NCSs despite the fact that all systems are causal due to the synthetic delay of 20 samples. So, the filter length has a major influence on the actuator placement which can be seen in **Figure 12**. The actuator position optimised with 100 filter weights has the highest filter quality of up to 400 filter weights, which means that the impulse response of the optimal filter has a short impulse response. So, it can be stated that a short filter leads to an actuator placement where a short impulse response of the optimal controller can be realised. This is the case if the secondary path is very similar to the primary path.

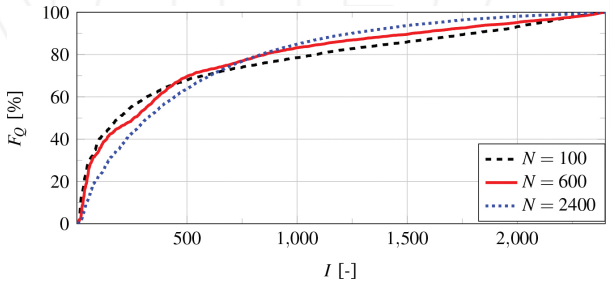

Figure 12. Filter qualities of the non-causal systems.

http://dx.doi.org/10.5772/64409

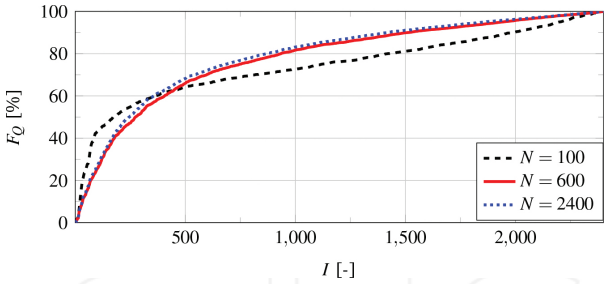

Figure 13. Filter qualities of the causal systems.

A comparison of the actuator positions of the CSs and the NCSs shows that the optimised actuator position for a short filter ($I = 100$) is the same for both systems. In contrast, the actuator positions for longer filters differ significantly between the two systems. To summarise, it can be said that the actuator position optimised with a short filter is not very sensitive to causality. Again, this matches Section 3.5., where it is shown that a time-advanced reference signal cannot be used for a system with a very short filter.

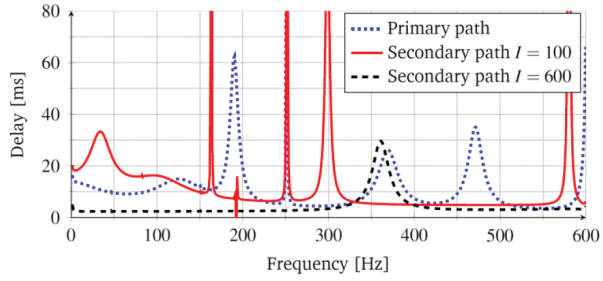

Figure 14. Group delays of the primary path and the causal system secondary paths.

For longer filters, the effect of the causality constraint becomes more pronounced. While the NCS was made causal by the synthetic delay induced in the primary path, the CS system is not causal if the actuator is located at the excitation point. So, in the case of the CS the causality constraint has to be fulfilled with a different actuator placement with smaller delays. This is achieved with the CS actuator placement with long filters. **Figure 14** presents the delays of the primary path and of the two secondary paths of the CSs (for $I = 100$ and 600).

By analysing the group delays it can be shown that the group delay of the actuator located near the error sensor has a smaller delay than the primary path. Only in the region of a non-minimum phase zero is the group delay higher than that of the primary path. In contrast, the actuator position near the excitation point has a larger group delay than the primary path nearly all over the frequency band, except some non-minimum phase zeros. The delay analysis clearly indicates that the causality constraint influences the actuator location for longer filters. Yet, because of the synthetic delay (17 ms) induced in the primary path, the causality constraint

does not affect the NCS locations. If the primary delay is 17 ms larger than the delay presented in **Figure 14**, the causality constraint is fulfilled even for the actuator located at the excitation point.

The last parameter investigated in this section is the influence of structural damping. In the case of higher structural damping, the vibration energy is not localised in the resonant frequencies and the filter effect of the structure is smaller. Accordingly, the deterministic parts of the disturbance signal are reduced and a non-causal actuator location has an even worse performance. This can be seen in **Figure 15**, which presents the optimised actuator locations for the CSs.

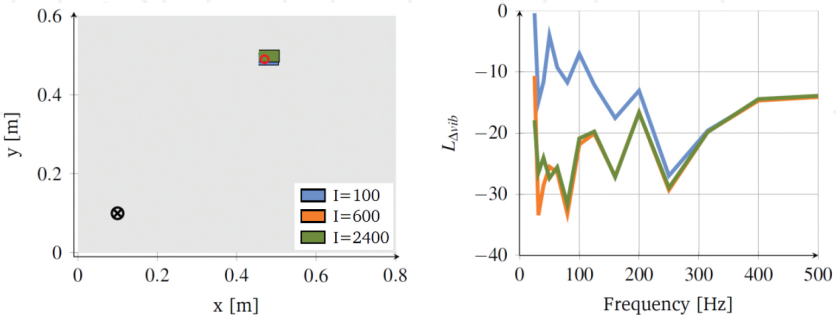

Figure 15. Optimised actuator positions for the causal system (left) with medium structural damping, vibration reduction at the error sensor in third octave bands (right).

In the case of medium structural damping, even the actuator optimised with 100 filter weights is located at the error sensor which is not the case for the light damping. This is due to the stronger performance penalties of the causality constraint for higher damped systems. A second tendency of the medium damped system can be seen on the right side of **Figure 15**. Compared to **Figure 10**, the performance for the higher structural damping is saturated with 600 filter weights. The need for less filter weights is due to the shorter impulse responses of the systems with higher structural damping.

4.3. Experimental validation

To experimentally validate the simulation results, two optimised actuator positions are realised on an aluminium plate. The experiments are focused on the different actuator positions caused by the variation of the filter length for the NCS configuration. The influence of the delays and the causality constraint was already shown by the author in [21] and is excluded in this investigation. For the experiments the actuator placements optimised with filter length of 100 and 2400 are realised.

The experiments are conducted on the test bed presented already in **Figure 1**. As it is presented in Section 3.2, a secondary path model and a synchronous measurement of the reference signal and the disturbance signal are required. Therefore, the piezoelectric patch actuator is driven

http://dx.doi.org/10.5772/64409

by band-limited white noise and the signal of the accelerometer and the disturbance are measured simultaneously. The time series are post-processed with a sub-space-based identification algorithm which identifies a state-space model [30]. Afterwards, the excitation shaker is driven with a band-limited white noise signal. The reference signal is measured with a load cell between the plate and the shaker and the disturbance signal is measured simultaneously at the accelerometer. All sensor signals are low-pass filtered and fed into a rapid prototyping DSP. The excitation is also realised with the DSP and fed to reconstruction low-pass filters. In **Table 4**, a complete list of the experimental hardware is presented.

Hardware	Type	Additional information
DSP	dSpace® ds1006	Sampling frequency: 1200 Hz
Low-pass filters	KEMO Card Master 255G	Cut-off frequency: 560 Hz
Accelerometer	PCB 352A24	Mass: 0.8 g
Shaker	LMS 201	
Piezoelectric patch actuator	PI DuraAct P-876.A15 (50 × 30 × 0.5 mm active area)	Mass: 10 g

Table 4. Experimental hardware.

After the offline calculation of the optimal filter, the filter weights are implemented in the DSP and the controlled performance can be measured. **Figure 16** presents the performance of the two actuator positions where two filters with 100 and 2400 weights are designed.

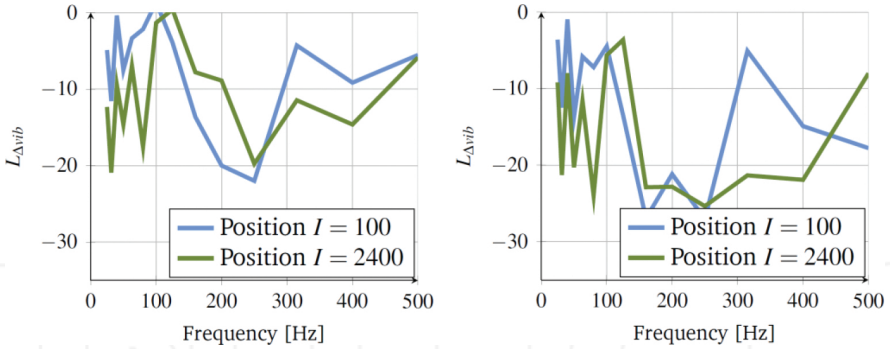

Figure 16. Experimentally measured vibration reduction in third octave bands of the two investigated actuator positions, with a filter length of 100 (left) and a filter length of 2400 (right).

In contrast to the simulation result, the actuator position optimised with 100 filter weights shows no performance advantages in comparison to the position optimised with 2400 filter weights. The opposite is the case for both filter lengths, the actuator position optimised with 2400 filter weights outperforms the position optimised with 100 filter weights. The total reduction of the feedforward controller using the actuator position optimised with 2400 filter weights integrated over the frequency band is 2 dB larger using in the case of an optimal filter with length 100 and 5 dB better using 2400 filter weights. This is indeed a surprising result.

This could be due to the model uncertainties shown in Section 2. Maybe, the optimisation with different filter weights is more sensitive to damping uncertainties. Another possible reason for this disagreement could be the simplified modelling of the piezoelectric patch actuators which maybe influence the performance of the feedforward controller especially in the lower frequency range. Nevertheless, the filter qualities for the different actuator positions fit the simulated ones. **Figure 17** shows that the actuator position optimised with 100 filter weights has a higher filter quality for short filters than the position optimised with 2400 filter weights.

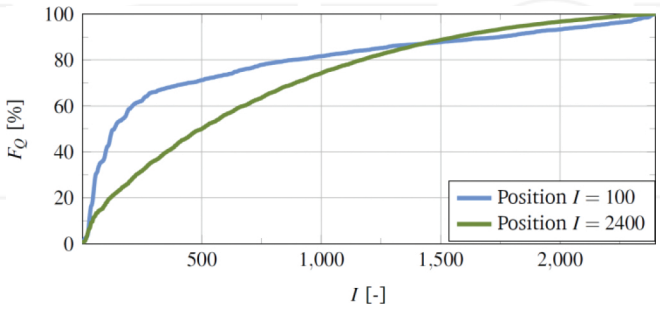

Figure 17. Filter qualities of the filters used in the experimental investigations.

In short, further investigations have to be done to investigate the dependency of the optimal actuator placement on the filter weights. In particular, the influences of the structural damping or other model uncertainties have to be shown.

5. Conclusion

This chapter presents and analyses the parameters influencing the performance of a feedforward control system. To this end, the basic theory of feedforward control systems is presented and the parameters (causality, FIR filter weights, saturation, etc.) which are necessary to design technical feedforward systems are studied. Furthermore, an extensive parametric study is presented in which the influence of each parameter is analysed. Therefore, each parameter is varied in a wide range. This chapter also shows the importance of modelling these parameters inside an actuator placement optimisation routine. During the optimisation, the influence of causality, the filter weights and the damping properties of the structure on the actuator placement is analysed.

It is shown that the causality constraint and the length of the FIR filter are of crucial importance for the feedforward control performance. A very short filter and large delays in the secondary path can significantly reduce the performance of a feedforward controller. Furthermore, the effect of structural damping on the performance is analysed. Under non-causal conditions, a larger structural damping leads to a decreased performance because the filtering effect of the

http://dx.doi.org/10.5772/64409

structural resonances is reduced and so are, as a consequence, the deterministic properties of the disturbance signal. In addition, the effects of a limited actuator performance (i.e. saturation effects) and the use of an overdetermined (rectangular) system (i.e. more sensors than actuators) are studied. It is shown that saturation and over determinacy lead to a performance cut-off.

After the analysis of the parameters, an actuator placement optimisation is presented that incorporates the analysed parameters of a feedforward control system into the actuator placement. The cost function of the optimisation is chosen to be the flexural vibration at a fixed error sensor so as to ease the analysis of the optimisation result. It can be shown that the actuator position is dependent on the delays that determine the causality as well as on the filter length. For very short FIR filters, the actuator is located at positions at which the optimal control filter has a short impulse response and thus compensates the filter length. Only if the filter length is extended to a certain level, the causality aspect influences the actuator positions. The influence of the causality aspect on the actuator placement increases with a higher structural damping.

In the experiments, the simulated influence of the filter weights on the actuator positions cannot be validated. The filter qualities of the investigated actuator positions equals the ones that are simulated, but the overall performance are not in agreement with the simulations. Further studies should investigate if the model uncertainties are the reason for the deviations.

To summarise, it is shown that the design of a feedforward controller is highly dependent on the considered realisation. It is important to know which time-advance can be gathered by the reference signal (for causality aspects), which length of the FIR filter can be realised with the chosen digital signal processor, etc. An optimisation of the actuator and sensor positions is only effective if these aspects are known.

In future studies, the optimisation of actuator and sensor locations for global cost functions such as global vibration or sound power reduction will be investigated. When using global cost functions, further parameters need to be considered for the optimisation of sensor and actuator positions for feedforward control systems. Research should focus, for example, on the pinning effect and the number of sensors and actuators.

Author details

Thomas Haase

Address all correspondence to: thomas.haase@dlr.de

1 German Aerospace Center (DLR), Institute of Composite Structures and Adaptive Systems, Lilienthalplatz, Braunschweig, Germany

2 Technische Universität Braunschweig, Institut für Adaptronik und Funktionsintegartion (iAF), Langer Kamp, Braunschweig, Germany

References

[1] Padula S.L., Kincaid R.K. Optimization strategies for sensor and actuator placement. NASA Center for AeroSpace Information (CASI). 1999, 17 p.

[2] Frecker M.J. Recent advances in optimization of smart structures and actuators. Journal of Intelligent Material Systems and Structures. 2003;14:207–216.

[3] De Fonseca P., Sas P., Van Brussel H. A comparative study of methods for optimising sensor and actuator locations in active control applications. Journal of Sound and Vibration. 1999;221:651–679.

[4] Gupta V., Sharma M., Thakur N. Optimization criteria for optimal placement of piezoelectric sensors and actuators on a smart structure: a technical review. Journal of Intelligent Material Systems and Structures. 2010;21:1227–1243.

[5] Clark R.L., Fuller C.R. Optimal placement of piezoelectric actuators and polyvinylidene fluoride error sensors in active structural acoustic control approaches. The Journal of the Acoustical Society of America. 1992;3:1521–1533.

[6] Gawronski W.K. Advanced Structural Dynamics and Active Control of Structures. 1st ed. New York: Springer; 2004.

[7] Wang B.-T. Optimal placement of microphones and piezoelectric transducer actuators for far-field sound radiation control. The Journal of the Acoustical Society of America. 1995;5:2975–2984.

[8] Nijhuis M.O., de Boer A. Optimization strategy for actuator and sensor placement in active structural acoustic control. In: International Symposium on Active Control of Sound and Vibration, ACTIVE, July 15–17, 2002, Southampton, UK (pp. 621–632).

[9] Kim J., Varadan V.V., Varadan V.K. Finite element-optimization methods for active control of radiated sound from a plate structure. Journal of Smart Materials and Structures. 1995;4:318–326.

[10] Moshrefi-Torbati M., Keane A., Elliott S.J., Brennan M., Anthony D., Rogers E. Active vibration control (AVC) of a satellite boom structure using optimally positioned stacked piezoelectric actuators. Journal of Sound and Vibration. 2006;292:203–220.

[11] Montazeri A., Poshtan J. Optimizing a multi-channel ANC system for broadband noise cancellation in a telephone kiosk using genetic algorithms. Shock and Vibration. 2009;16:241–260.

[12] Belgacem W., Berry A., Masson P. Active vibration control on a quarter-car for cancellation of road noise disturbance. Journal of Sound and Vibration. 2012;331(14):3240–3254.

[13] Kuo S.M., Morgan D.R. Active Noise Control System: Algorithms and DSP Implementations. 1st ed. New York: John Wiley & Sons, Inc.; 1996.

[14] Nelson P.A., Elliott S.J. Active Control of Sound. London: Academic Press; 1991.

[15] Burdisso R., Vipperman J., Fuller C. Causality analysis of feedforward-controlled systems with broadband inputs. The Journal of the Acoustical Society of America. 1993;94:234–242.

[16] Haase T., Algermissen S., Unruh O., Misol M. Experiments on active control of counter-rotating open rotor interior noise. Acta Acoustica United with Acustica. 2014;100:448–457. DOI: 10.3813/AAA.918725.

[17] Miller S., Shipps J.C. Active noise cancelling muffler. US-Patent. 1998; Patent Number: US5748749A.

[18] Hammerschmidt C. Active noise cancellation applied to diesel exhaust, 2010, [Internet]. Avaiable form: : http://www.eetimes.com/document.asp?doc_id=1257672 [Acessed: 22.06.2016].

[19] Elliott S.J. Signal Processing for Active Control. 1st ed. London: Academic Press; 2001. 511 p.

[20] Widrow B., Stearns S., Stearns P.N. Adaptive Signal Processing. 1st ed. Englewood Cliffs, NJ: Prentice Hall; 1985. 485 p.

[21] Haase T., Misol M., Rose M. Optimal placement of flat piezoceramic actuators for feedforward systems under the influence of real-time hardware delays. Journal of Sound and Vibration. 2015;345:34–46.

[22] Janocha H., Liu B. Simulation approach and causality evaluation for an active noise control system. IEE Proceedings in Control Theory and Applications; IET. 1998;145(4): 423–426.

[23] Minkoff J. The operation of multichannel feedforward adaptive systems. IEEE Transactions on Signal Processing. 1997;45(12):2993–3005.

[24] Rose M. Modal based correction methods for the placement of piezoceramic Modules. In: ASME International Mechanical Engineering Congress and Exposition. 05 November 2005; Orlando, Florida, USA; 2005.

[25] Lee K.-A., Gan W.-S, Kuo S.M. Subband Adaptive Filtering: Theory and Implementation. 1st ed. West Sussex, UK: John Wiley & Sons Ltd.; 2009.

[26] Pohlheim H. Evolutionäre Algorithmen. 1st ed. New York: Springer; 2000. DOI: 978-3-642-57137-4.

[27] Pohlheim H. GEATbx: Genetic and evolutionary algorithm toolbox for use with MATLAB [Internet]. 2006. Available from: http://www.geatbx.com/docu/ [Accessed: 10.11.2011].

[28] Unruh O., Haase T., Pohl M. Application of a load-bearing passive and active vibration isolation system in hydraulic drives. In: MOVIC/RASD Conference Proceedings; 3–6 July 2016; Southampton, UK; 2016.

[29] Kessissoglou N.J., Ragnarsson P., Löfgren A. An analytical and experimental comparison of optimal actuator and error sensor location for vibration attenuation. Journal of Sound and Vibration. 2002;260:671–691.

[30] Kateyama T. Sub-space based identification algorithms. 1st ed. New York: Springer; 2005.

[31] Wang W.Y., Yue K., Shi D.Y. Optimal research of actuator placement for piezoelectric smart structure. Journal of Key Engineering Materials. 2010;419:173–176.

[32] Preumont A. Vibration Control of Active Structures. 1st ed. Dordrecht: Kluwer Academic Publishers; 1997.

[33] PI Ceramic. DuraAct Flaechenwandler [Internet]. 2015. Available from: http://www.piceramic.de/produkt-detailseite/p-876-101790.html [Accessed: 02.02.2015].